PCCP

Accepted Manuscript

ROYAL SOCIETY OF CHEMISTRY

www.rsc.org/pccp

Synthesis and Characterization of Octaarginine Functionalized Graphene Oxide Nano-carrier for Gene Delivery Applications

Rana Imani[†,‡], Shahriar Hojjati Emami[†,*], Shahab Faghihi[‡,*]

[†]*Department of Biomedical Engineering, Amirkabir University of Technology, Tehran15875/4413, Iran*

[‡]*Tissue Engineering and Biomaterials Division, National Institute of Genetic Engineering and Biotechnology, Tehran 14965/161, Iran*

[*]*Corresponding author:* Biomedical Engineering Department, Amirkabir University of Technology, Tehran 15875, Iran.
Tel.: +98 21 6454 2367; fax: +98 21 6646 8186.
E–mail address: semami@aut.ac.ir

[*]*Corresponding author:* Tissue Engineering and Biomaterials Division, National Institute of Genetic Engineering and Biotechnology, Tehran 14965/161, Iran.
Tel.: +98 21 44580386; fax: +98 21 44580386.
E–mail address: sfaghihi@nigeb.ac.ir, shahabeddin.faghihi@mail.mcgill.ca (S. Faghihi).

Abstract

The success of gene therapy is largely dependent on development of a gene carrier. Recently cell-penetrating peptides (CPPs) have been employed for enhancing gene and drug delivery efficacy of nano-particles. The feasibility of octaarginine (R8) functionalized graphene oxide (GO) as a novel nano-carrier for gene delivery is investigated. DNA plasmid expresses enhanced green fluorescence (pEGFP) is used as a model gene to study the R8-GO transfection ability into mammalian cells. Different ratios of R8 peptide (0.1-1.5 μmol per mg of GO) is conjugated to carboxylated graphene oxide by two steps amidation process. The process of peptide conjugation is analyzed by Fourier transform infrared (FTIR), atomic forced microscopy (AFM), Uv-vis spectroscopy and X-ray diffraction (XRD). In order to obtain the highest transfection of pEGFP into the cells, the amount of bonded peptide to GO is optimized which is evidenced by dynamic light scattering (DLS), zeta potential, TNBS and gel retardation assays. The cytotoxicity of R8-functionalizrd GO is also tested by MTT assay. The results confirm the successful attachment of R8 peptide to GO. The AFM and XRD results show significant increase in thickness of nano graphene oxide sheets (NGOS) from 0.8 to 2-7 nm as well as an increase in GO interlying space after R8-functionalization process. A reduction in nano-carriers stability in both aqueous solution and cell culture media are observed when the amount of peptide increased more than 1 μmol/mg. Gel electrophoresis analysis shows the highest DNA loading on the peptide functionalized GO at the ratios of 0.5 and 1 μmol/mg. As the result, the 1 μmol/mg of conjugated peptide sample shows the highest conjugational efficiency and EGFP gene expression along with improved dispersibility and biocompatibility. Overall, the findings reveal the importance of peptide density on the surface of NGOS in order to obtain the most efficient cell transfection. It is concluded that the R8-conjugated GO could be a promising delivery nano-carrier for gene delivery with relevancy in the biotechnology therapeutics and clinical applications.

Keywords: Gene therapy; Nano-carrier, Graphene oxide; Cell penetrating peptide; Octaarginine.

1- Introduction

To have a successful gene therapy a carrier that efficiently delivers nucleic acids into the cells is commonly required [1, 2]. One major obstacle that impedes a successful transfection of nucleic acid molecules is the development of a simple, safe, and efficacious delivery system. An ideal gene delivery carrier must compact genetic materials into nano-sized particles that are colloidally stable, protect nucleic acids from enzymatic degradation, effectively transit nucleic acids to target cells, and achieve a significant transfection yield [3].

In recent years, nanotechnology has revolutionized medical treatments and therapies particularly by gene delivery [4]. Various nano-materials with unique physical and chemical properties have been used in the field such as carbon-based materials [5, 6]. Graphene, a single layer of carbon atoms in a closely packed honeycomb two-dimensional structure, is a new kind of carbon nanostructure material which attracted many attentions [7]. Graphene and its derivatives such as graphene oxide (GO) possess unique characteristics including high water dispersibility, good colloidal stability, tunable surface, and good biocompatibility [8]. The abundant oxygen functional groups on the basal plane and edges of GO can be used as anchoring sites for bio-functionalization purposes (Schematic. 1a). These attributes make the GO more attractive and potent candidate rather than other nano-carriers [9]. In particular, the use of GO as a potential vehicle for targeted delivery of drugs and genes in cancer therapy has attained considerable interest [10]. Duo to the inherent negative charge of GO sheets, for an efficient gene delivery it is necessary to modify its surface in order to achieve effective loading of negatively charged genetic components such as plasmid DNA (pDNA), short interference RNA (siRNA), etc. A practical strategy to accomplish such complexion that enhances transfection ability of GO with no cytotoxic effect, could be incorporation of cationic molecules as a linker into the surface of GO [11].

Reports have explored the efficacy of various surface functionalization methods in order to improve the carrier ability of GO. Dai and colleagues have demonstrated that polyethylene glycol functionalized GO is able to deliver aromatic, water-insoluble anticancer drugs into cells [12]. The application of graphene as a transporter to deliver oligonucleotides for gene detection and therapy has been reported in few studies [13-15]. Feng et al. have successfully performed physical complexion of different molecular weights of polyethyleneimine (PEI) with GO as a nano-vehicle for gene transfection [16]. In the other studies, Kim et al. and Chen et al. have developed a GO-based gene delivery system by covalent conjugation of branched PEI to GO nano-sheets [13, 17]. Chitosan (CS) as a positively charged biopolymer has been utilized by Le and his co-workers to improve surface functionality of GO. They have shown that the GO-CS nano-carrier is able to carry and deliver both anticancer drugs and genes [18]. The polyethylene glycol conjugation along with π-π stacked pyrenemethylamine have been employed for surface functionalization of GO to deliver siRNA to cancer cells [19].

Recently, cell penetrating peptides (CPPs) have gained much attention due to their ability to translocate drugs, genes, and large therapeutic molecules intracellularly [20]. CPPs are short strands of arginine and/or lysine-rich peptides (<30 amino acids) that use their cationic nature for efficient intracellular accumulation. It has been reported that these kinds of peptides may enhance cellular uptake owing to their strong tendency for cell adherence, without any dependency on receptors, temperature, nor an energy-dependent pathway [21]. One such example is arginine (R) rich CPP like TAT peptide (derived from the HIV-1 protein) or octaraginene (R8). These peptides are small, highly cationic and have the ability to cross the plasma

membrane of eukaryotic cells [22]. Among all the polyarginine peptides, the R8 (Schematic. 1b) has shown the highest cellular uptake while R6 and R9 presented optimum translocation through cell membrane [23]. It is shown that the transduction efficacy of different nano-particles or biomolecules (e.g. proteins, nucleic acids) into cells can be improved using R8 peptide because of its natural based composition and low cytotoxicity [24]. While much research has been devoted to the functionalization of nano-particles with R8 peptide for variety of applications there has been no investigation on R8-conjugated GO nano-sheets as a potential gene carrier.

In this study, a novel CPP-conjugated GO, as gene carrier system was strategically designed and prepared. We aimed to improve the transfection efficiency of nano-graphene oxide sheets (NGOS) by R8 conjugation while maintaining a low cytotoxicity. The effect of conjugation ratio (R8 to GO) on the surface charge, particle size, morphology, and DNA complexion ability of the nano-carriers was also investigated. The optimized nano-carrier formulation was achieved after a precise chemical, physical and biological characterization.

2. Materials and methods

2.1. Materials

All chemical materials involved in GO synthesis were purchased from Aldrich (Japan). Octaarginine was obtained from GL Biochem LTD (Shanghai). DMEM culture medium, fetal bovine serum (FBS), Trypsin, MTT solutions and phosphate buffer solution were all purchased from GIBCO (UK). The L929 fibroblast and HEK cell lines were obtained from American Type Culture Collection (ATCC, Manassas, VA, USA). Plasmid DNA encoding enhanced green fluorescent protein (pEGFP) was purchased from Invitrogen (USA). Sodium bicarbonate, sodiumdodecyl sulfate (SDS) and 2,4,6-Trinitrobenzene sulfonic acid (TNBS) used for TNBS assay were purchased from Merck (Germany).

2.2. Methods

2.2.1. Preparation of nano-graphene oxide sheets (NGOS)

The NGOS was prepared based on a modified Hummer method[25]. In a typical experiment, natural graphite powder (1 gr) was suspended in 120 ml of sulfuric acid (98%). The mixture was cooled in an ice bath followed by addition of $NaNO_3$ (500 mg) under moderate stirring (200 RPM). After 60 min $KMnO_4$ (6 gr) was added and the mixture was heated to reach 35 ºC under constant stirring condition. After 48 hours, the brownish green solution became too viscose to stir. Double distilled water (DDW) was slowly added to the reaction to keep the temperature at 70 ºC for one hour. Finally, 30% H_2O_2 (10 ml) was added to the mixture until the color was changed to bright yellow. The mixture was rested for 2 days to precipitate GO nano-sheets. The supernatant was removed and precipitated powder was washed ten times with 0.5 M aqueous HCl to remove metal ions followed by washing with DDW to remove the acid residues. To achieve nano-sized mono layer GO sheet, the suspension was dispersed by probe-typed ultrasonic treatment (200 W, 2h). The resultant brown solution was freeze dried to obtain a fine nano-graphene oxide powder.

2.2.2. Carboxylation of nano-graphene oxide sheets (NGOS-COOH)

Carboxylic acid functionalized nano-graphene oxide sheets (NGOS-COOH) was obtained through reaction with chloroacetic acid under strong basic conditions to transform the hydroxyl, epoxide, and ester groups into carboxylic acid (COOH) moieties. The carboxylation process was performed under optimized condition based on our previous study. Briefly, 1mg of NGOS was

dispersed in deionized water (1ml) under probe-type sonication (100W, 30 min) to obtain a clear solution. Chloroacetic acid solution in 4M NaOH was prepared and the NGOS aqueous suspension was immediately added to the final concentration of 0.2 mg/ml. The suspension was reacted for 75 min (or 12h) under bath-sonication at room temperature to transform -OH groups to -COOH via conjugation of acetic acid moieties. The NGOS-COOH solution was centrifuged and washed five times with DDW and transferred to a dialysis bag. After dialysis against DDW to remove the excess reactant, a well dispersed NGOS-COOH aqueous solution was obtained.

2.2.3. Peptide conjugation

The synthesized nano-carrier (NGOS-COOH) was functionalized by octaarginine peptide sequence (R8) through two steps diimide-activated amidation under ambient conditions[26]. In the first step, 10 mg of NGOS-COOH was suspended in 10 mL of deionized water by sonication of the mixture for 1 h. Subsequently, 5 mL of a 500 mM MES buffer solution (pH ~ 6.1) and 5 mL of a 50 mg/ mL NHS aqueous solution were added to the above mentioned suspension. After 15 min of fast stirring, 6 mL fresh EDAC aqueous solution (10 mg/mL) was added to the mixture at room temperature. After 30 min stirring the suspension was centrifuged and rinsed thoroughly with 50 mM MES buffer solution (pH ~ 6.1) to remove excess reactants. In the second step, the estered nano-sheets were re-dispersed in 5 mL of 50 mM MES buffer solution (pH ~ 6.1) and 1mL of R8 in MES buffer solution (pH ~ 6.1) was added to the mixture. After shaking the mixture on a platform shaker (150 rpm) at room temperature for 24 h, the suspension was centrifuged and washed with MES buffer solution to remove unbounded proteins. The peptide functionalized nano-sheets were dispersed in deionized water for further measurements. A series of peptide-NGOS complexes was obtained using various R8:NGOS ratios (μmol:mg) consists of 0.1, 0.5, 1 and 1.5. The samples were called GOP0.1, GOP0.5, GOP1 and GOP1.5, respectively.

2.3. Nano-carriers characterization

2.3.1. Instrumentation

The samples including NGOS, NGOS-COOH, and R8-functionalized NGOS were pressed into the potassium bromide pellets and examined with Fourier transform infrared (FTIR) spectrophotometer within the range of 3600–500 cm^{-1} at a resolution of 4 cm^{-1} (German Nicolet FTIR Nexus-670 IR). Uv-vis absorption spectra of the samples were also obtained using a Neosys-2000, Scinco Co. Ltd., Korea spectrophotometer at room temperature. The size and morphology of NGOS, NGOS-COOH and R8-NGOS samples deposited from a dilute aqueous dispersion (0.01mg/ml) on a freshly cleaved mica were determined by an atomic force microscope (AFM, Nanoscope III Multimode,VEECO) in tapping mode and transmission electron microscope (TEM, Philips169 CM200 200 kV). The X-ray diffraction (XRD) analysis of the samples was performed using a diffractometer (EQUINOX300, Inel, France) at 2θ ranging from 5˚ to 40˚ using CuKα radiation (40kV, 100mA). Finally, zeta potential of the samples (0.01mg/ml, pH 6.1) as well as hydrodynamic size distribution were measured using a Zetasizer Nano-ZS-90 (Malvern Instruments, UK).

2.3.2. TNBS assay

For quantification of attached R8 peptides to graphene nano-sheets' surface a colorimetric-based assay was used which employed 2,4,6-Trinitrobenzene sulfonic acid (TNBS, Thermo Scientific Pierce). The R8 peptide solutions were first used to produce a standard curve for quantification of R8 binding onto the graphene nano-sheets. In brief, 0.5 mL TNBS in 0.1 M

sodium bicarbonate (pH 8.5, 0.01%, w/v) was added to 1 mL of R8 solutions having different concentrations (10 to 100 μg/mL). The mixtures were then incubated at 37 °C for 2 h followed by the addition of 0.5 mL of 10% sodiumdodecyl sulfate (SDS) and 0.25 mL of 1 M HCl to each solution. The absorbance was read at 335 nm and plotted against R8 concentration for each sample. After the addition of peptide conjugated samples (0.5 mg/mL) to TNBS solution, the peptide concentration per mg of GO nano-sheets was calculated for each sample (Schematic 2).

2.3.3. Cell culture and cytotoxicity assay

L929 fibroblast cells were cultured in Dulbecco's modified eagle medium (DMEM) containing 10% fetal bovine serum (FBS), streptomycin (100 μg/ mL), penicillin (100 μg/ mL), at 37 ˚C in a humidified 5% CO_2-containing atmosphere. The cytotoxicity of different samples in comparison with NGOS, R8 and PEI as controls was evaluated using MTT assay. Briefly, the fibroblast cells were seeded in a 96-well plate at a density of 10^4 cells/well. After 24 h incubation, the culture media were replaced with 100 μL of fresh media containing the samples. After an additional 24 h, the cells were washed with PBS and 20 μL of MTT (5mg/mL) solution in phosphate buffered saline (PBS) was added to each well and incubated for another 4 h. The supernatant was then removed and the formazan crystals were dissolved in DMSO (100 μL per well). The absorbance was read at 570 nm by a micro-plate reader (Model 680 Bio-RAD) and reported as the percentage of cell viability compared to the controls.

2.3.4. In vitro gene transfection assay

A DNA plasmid encoding enhanced green fluorescence protein (EGFP) is used as a gene model to study the transfection ability of peptide-functionalized samples. The reporter plasmid pEGFP was transformed in E. Coli DH5a and was amplified in Luria–Bertani (LB) medium at 37˚C overnight at 250 rpm. The plasmids were purified by a high pure plasmid isolation kit (Roche, Germany) according to the manufacturer's protocol. The concentration and purity of plasmids were determined by UV absorbance measurements at 260 and 280 nm. The plasmids were preserved at -20˚C prior to use.

Before *in vitro* gene transfection experiment, the pDNA loading and complexion capability of synthesized nano-carriers was investigated by gel retardation assay. Complexes of pDNA with NGOS, GOPs, and different concentration of pure peptides were prepared by the addition of sample suspensions (10 μL) to the pDNA solution (10 μL) followed by 30 min incubation at room temperature. The complexes were then electrophoresed through a 1% (w/v) agarose gel containing ethidium bromide (EtBr, 0.5 μg/mL) in 0.5 TAE (Tris -acetate-EDTA) buffer at 100 V for 30 min. The gel was subsequently analyzed on a UV illuminator (wise UV WUV, DAIHAN Scientific, Seoul, Korea).

In vitro transfection experiment of R8-NGOSs was qualitatively assessed against HEK 293 (Human Embryonic Kidney 293) cells by fluorescence microscopy. The cells were cultured in a 24-well culture plate at an initial density of 3×10^4 cells/ml and incubated for 24 h. Under a mild pipetting condition, 10 μL of each sample (100 μg/mL) which was diluted in 100 μL of serum free media was mixed with 1 μg of pDNA (10 μL) and incubated for 30 min at room temperature for complexion. The cells were then incubated with each complex in 250 μL serum free media for 5 h, followed by 18 h incubation in 750 μL of FBS containing media. Pure R8 peptide and PEI (10^4 g/mol) with the concentration of 100 μg/mL were used as controls. The transfection of the cells was analyzed by a fluorescence microscope (TCS SP5 Leica).

Besides fluorescent imaging, to quantitatively evaluate gene transfection ability of optimized nano-carrier and to study the effect of serum on transfection efficacy, intensity of GFP expression was measured after 48 h transfection by a Microplate Reader (SpectraMax i3 Multi-Mode, Molecular devices). Briefly, 250ng of pEGFP was mixed to 10 µL of GOP1 (50µg/mL) according to the same procedure as above. HEK 293 cells were seeded in 96-well plates (100µL media+10% FBS), 24 h prior to transfection assay. The media was removed then and the cells were washed with PBS. Subsequently, 100µL DMEM (in presence and absence of serum protein, FBS) contained complexes was gently added to the cells. After 8 h of incubation, the transfection medium was removed, and 200µL fresh media (DMEM containing 10% FBS) was added for another 40h incubation. Finally, cells were washed with PBS (3 times) and the fluorescent intensity of GFP was read by a micro-plate reader (excitation: 480nm, emission: 520 nm). As for controls, the cells without any treatments, cells treated by JetPEI® (Poluplus transfection Inc , New York) and cells treated by naked pEGFP (250 ng) were used as blank sample, positive control and negative control, respectively. The relative transfection ability of the samples was expressed as relative fluorescence intensity calculated based on equation (1):

$$\text{Relative Fluorescence Intensity} = (E_t - E_b) / E_{c+} \qquad \text{Eq. 1}$$

Where E_t, E_b and Ec_+ represent average fluorescence emission of test samples, blank sample and positive control (JetPEI®,+FBS), respectively.

2.4. Statistical analysis

Statistical analysis was carried out using SPSS software (v 17.0; IBM New York, NY, USA). Data were first analyzed by analysis of variance (ANOVA); when statistical differences were detected, a Tukey's Multiple Comparison test was performed. Data are reported as mean ±SD at a significance level of $p < 0.05$.

3. Results and discussion

3.1. FTIR spectroscopy

The chemical structure of synthesized NGOS, NGOS-COOH and R8-functionalized NGOS samples were characterized by FTIR spectroscopy (Fig.1). The FTIR analysis demonstrated the successful synthesis of NGOS. The appearance of characteristic absorption peaks at 3410, 1733, 1620 and 1520 cm^{-1} revealed the presence of OH, C=O, COOH and C=C functional groups in NGOS, respectively. After chloroacetic acid activation, the resulting NGOS-COOH derivative showed a stronger absorption band at 1620 cm^{-1} which is an indication for the formation of more carboxylate moieties. The peak at ~1230 cm^{-1} is attributed to the vibration mode of epoxide groups (C–O–C) which is more pronounced in the NGOS spectra compared to carboxylated samples where the peak is almost vanished. This is possibly duo to the synergistic effects of chloroacetic acid on both epoxide and hydroxyl groups. After NGOS reaction with chloroacetic acid, two strong peaks at 2854 and 2925 cm^{-1} were appeared which are correlated to the symmetric and asymmetric stretching modes of $-CH_2-$ groups in chloroacetic acid. The peak at 1390-1400 is also attributed to the deformation vibration of $-CH_2-$ group [27].The small peak at ~2360 cm^{-1} is associated to the O−H stretch from strongly hydrogen-bonded −COOH which could confirm the chemical attachment of many $–O-CH_2-COOH$ to the NGOS sheets [28].

After conjugation of R8 peptide to the NGOS-COOH, a characteristic band at 1742 cm^{-1} (stretching vibration of CONH) was appeared which indicated the successful formation of R8-NGOS. This was also confirmed by the appearance of two main characteristic peaks of

octaarginine at 1463 cm^{-1} (amide II) and 1651 cm^{-1}. The prominent peak at 1667 cm^{-1} is assigned to guanidine C=N stretching and C=O carbonyl stretch of octaarginine whereas the peak at 1139 cm^{-1} is attributed to C–N stretching. The N-H stretching of primary and secondary amine groups of guanidine were presented near 3100-3500. The comparison between the FTIR spectra before and after R8 conjugation to the NGOS confirmed the successful binding of octaarginine to the nano-carriers as the amide group peaks of R8-NGOS were appeared (Fig. 1).

3.2. Uv-vis spectroscopy

The peptide functionalized NGOS was further characterized by Uv-vis spectroscopy. As shown in Fig. 3a, the NGOS showed a characteristic peak at 231 nm corresponds to π-π* transitions of C=C bonds as well as a shoulder at 300 nm corresponds to σ-π* transitions of carboxyl bonds. The carboxylated sample showed a much higher absorbance in the Vis-NIR range as compared to the NGOS. The significant increase in the absorbance was led to a darkening of the solution which can clearly be seen with the eye (Fig. 3a, inset) [4, 6]. The Uv-vis spectrum of R8 solution (0.01 mg/mL) showed a characteristic peak at ~208 nm which is correlated to guanidine group of R8 (Fig. 3b). The R8-NGOS showed both dominant peaks of graphene oxide and R8 around 240 and 200 nm, respectively. The shift of these peaks is attributed to the amidation and reduction of NGOS after the R8 peptide conjugation [30, 31].

3.3. XRD analysis

The distances between the sheets as well as their folding and structural disruptions in graphite and its functionalized derivatives are highly different [27]. Therefore, the graphite, NGOS, carboxylated and peptide functionalized samples were characterized by XRD for more structural analysis. The XRD patterns confirmed the chemical oxidation of the exfoliated graphite and formation of GO sheets (Fig. 3c). The typical diffraction peak of native graphite was observed at 2θ= 26.8. The oxidation process was resulted in the formation of hydroxyl and epoxy groups as well as carboxyl groups mainly located on the center and lateral sides of the sheets, respectively. The inclusion of these functional groups resulted in a weakening of *van der Waals* force between the graphene sheets in the exfoliated GO. The appearance of diffraction peak of NGOS at 2θ = 12.3 with no reflection at 2θ=26.8 indicated that the exfoliation process under strong acidic condition had increased the sheets spacing [7]. Further carboxylation process under basic condition was resulted in a more dispersion and exfoliation of nano-sheets probably duo to the addition of chloroacetic acid residue (–O-CH_2-COOH). As the result, the carboxylated sample showed much weaker and broader diffraction peak at 2θ=12.3 as compared to the NGOS which indicates an increase in the interlayer spacing. For R8-functionalized sample, the weakest diffraction peak was detected at 2θ=12.6 which is corresponded to a slightly higher d-spacing rather than that of the NGOS-COOH. It is evident that the increase in the interlayer spacing between GO sheets is because of functionalization of graphene sheets by R8 molecules.

3.4. Size and morphology analyses

The size and morphology of NGOS, NGOS-COOH and R8-conjugated samples having various conjugation degrees were investigated by AFM and TEM. The AFM images of as prepared NGOS indicated a sheet-like morphology with the size of 250-400 nm. The AFM was used more for lateral size and thickness measurement of nano-sheets. Based on our AFM data, the nano-sheets appeared to be highly varied in shapes and lateral sizes. However, the z-section analysis for thickness measurement of nano-sheets after chloroacetic acid treatment and R8 conjugation showed a consistent results and confirmed sheets exfoliation and peptide

conjugation, respectively. The thickness of unmodified NGOS which measured from the height profile of the AFM image was about 1-1.5 nm. This thickness is corresponded to 1-2 layered graphene sheets (Fig. 2a). Modification of NGOS using chloroacetic acid followed by peptide conjugation changed nano-sheet thickness (Fig. 2b,2c). The carboxylated sample mean thickness was about 0.8 nm indicating the formation of a single layered sheet (Fig. 2b). The TEM analysis provided more detailed morphological insight on the samples (Fig. 2d). Based on the TEM images, typical wrinkle morphology for the GO and its exfoliation into a single or very thin layer after carboxylation treatment was observed. The smaller size of the carboxyl functionalized sample could be caused by the sonication process which was involved in the activation step. Duo to the strong basic condition of carboxylation process, the modified samples showed reduced size of 100-200 nm [29]. The size reduction of carboxylated GO could be more attractive for biological interactions particularly gene and drug deliveries where a larger surface area is necessary for biomolecular conjugation.

The DLS measurement was also used for an estimation and comparison of size alteration among the samples as the concentration of the peptide increased (Table 1). Before running DLS, to remove large non-uniformed nano-sheets observed by AFM, the NGOS and NGOS-COOH as-prepared solutions centrifuged for 5 min (14000 rpm). This could be the reason that DLS showed smaller average size for NGOS and NGOS-COOH compared to AFM analysis. However, the DLS characterization could not reveal the accurate size of nano-sheets in aqueous solution, as it considers the GO sheets spherical in shape whereas they are more accurately 2-D objects. Therefore, the average nano-sheets diameter reported from DLS is rather the effective hydrodynamic diameter of an equivalent sphere described by the tumbling of the nano-sheets. Additionally, even though GO nano-sheets seems rigid when deposited on an atomically flat surface (for the AFM experiment), in reality they are highly pliant sheets that could easily conform to any figure on that surface.

The height topographical study of R8-NGOS by AFM indicated that the peptide chains were successfully grafted onto the surface of GO sheets. Interestingly, the peptide grafted samples showed a reduced size of 50-100 nm and increased thickness of 3-7 nm. After the covalent modification of GO with R8, many protuberances were observed on the surface of nano-sheets that suggests immobilization of a large amount of peptides onto the basal plane of GO sheets. The most of R8-conjugated nano-sheets showed domed morphology while GO sheets showed very sharp edges with flat surface. In contrast, on non-carboxylated samples (NGOS), most of the peptide chains seem to graft on the basal parts of the sheets rather than the edges (Fig. 2c).

The increase in the peptide to GO ratios from 0.1 to 1.5 showed to gradually increase the thickness of the samples from 3 to 10 nm. For GOP1 sample, the AFM image indicated a successful peptide conjugation on the single sheet.

3.5. TNBS assay

In non-viral based gene delivery, one of the least studied areas which may directly affect cellular uptake efficacy is the influence of peptide density on nano-carriers. Khalil et al. have shown that the density of R8 peptide on liposomal nano-carrier would affect the uptake mechanism which directly influence the intracellular trafficking and results in different levels of gene expression [35]. In order to quantify the R8 peptides molarity on the R8-functionalized NGOS samples, TNBS assay was used. The TNBS would react with primary amino groups of amino acids in aqueous solution (pH=8) and form a yellow component which can be detected at 345 nm

(Schematic 2). It should be noted that the guanidine amine groups react with TNBS at slower rate than primary N-terminal amine groups.

To quantify the peptide functionalization efficacy, the absorbance value of the samples after interaction with TNBS solution was read and compared using a plotted standard curve (Fig. 5). The measurement was performed comparatively to optimize the reaction condition among the samples. However, ideally, it would be more relevant to use N-terminally acetylated analog of the R8 peptide to prepare calibration curve. The results confirmed the binding of the peptide chains on the GO nano-sheets. The amount of bonded R8 peptides (μmol/mg) and conjugation efficacy were calculated and listed in Tables 2. It can be seen that the amount of bounded peptide is proportional to the initial concentration of peptide being used. As the initial amount of peptide increased, the GOP1 showed the highest conjugation efficacy among the samples. However, the conjugation efficacy decreased in GOP1.5 rather than GOP1. It is therefore essential to optimize the conjugation process in term of the amount of bonded peptide molarity per mg of GO nano-sheets.

3.6. Zeta potential and dispersion stability analyses

Zeta potential is an important factor for characterization of dispersion stability of colloidal systems. It is directly influenced by the electrostatic interaction between different functionalized graphene sheets and other biomoleculs [30]. The surface charges of the NGOS before and after carboxylation process with chloroacetic acid were determined (Table. 1). As depicted in table 1, the activation of graphene oxide sheets by chloroacetic acid under basic condition decreased zata potential of NGOS due to the introduction of more carboxylic groups. This is advantageous as it provides a better condition for subsequent peptide conjugation. Furthermore, due to the hydrophilic nature of the carboxylated graphene nano-sheets, the dried powder can readily be exfoliated in water and form a stable colloidal suspension under a mild sonication treatment. The carboxylated sample was highly dispersed even after 3 months without any precipitation whilst unmodified NGOS underwent colloidal instability after this period of time. There was no significant change in NGOS-COOH size even after 3 month incubation (93±4.3 compared to 85±2.5), whereas for the untreated GO, a significant increase in size was detected by DLS measurement (478 ± 33 compared to 110±6).

The zeta potential measurement was also carried out on the peptide functionalized GO samples having different amounts of the R8 peptide. The results showed that by conjugation of R8 on the graphene nano-sheets zeta potential was significantly increased which is a confirmation on the addition of positively charged amine groups of R8. It was revealed that the R8:GO ratios of 0.5:1, 1:1 and 1.5:1 resulted in a significant increase in zeta potential as compared to the NGOS-COOH.

An increase in size was detected when the amount of R8 peptide increased from 0.5 to 1 μmol/mg. The size increase was significant when the amount of R8 peptide was enhanced from 1 to 1.5 μmol/mg. However, a significant increase in size distribution was detected for GOP1.5. This result is confirmed by the instability test observed for GOP1.5 which presented a partial aggregation during incubation at room temperature (Fig. 4). The stability of the peptide-functionalized NGOS was also analyzed by DLS measurements (Table 3). It is demonstrated that for GOP0.1, GOP0.5 and GOP1 there was no significant size alterations during incubation in deionized water or culture media (DMEM+10% FBS) after 48 h which indicates a good colloidal stability of prepared nano-carriers. However, all the samples showed slight size increase after 1h

incubation in culture media compared to deionized water which could be duo to surface absorption of serum proteins [32]. A significant instability was observed for the GOP1.5 sample even after 6 h incubation in culture media (Fig.4). After 48h, the aggregates were large enough to sediment and their size was around 1μm and 800 nm in DMEM and DI water, respectively (Table 3).

The results of TNBS assay and zeta potential analysis revealed that as the concentration of the peptide increased (from GOP0.1 to GOP 1.5) the amount of conjugated peptide and the positive charges increased. However, gel electrophoresis data showed less DNA condensation in GOP1.5 compared to GOP1. We speculated that the extra peptide chains could bridge between two or more nano-sheets and cause inter-particle crosslinking as the concentration of peptide increased. Although there is no chemical evidence to confirm whether the peptide-mediated cross-linking is due to covalent binding or physical interactions, based on the DLS results it is apparent that the inter-particle crosslinking of GOP1.5 nanoparticles is mostly covalent. Size and polydispersity index (PDI) analyses immediately after a harsh sonication process showed a significant increase as the concentration of peptide enhanced from GOP1 to GOP1.5 suggesting a larger particle size distribution. The non-uniformed size distribution for GOP1.5 suggests formation of some nano-clusters (resulted from peptide mediated covalent cross linking). Although the guanidine amine groups are less reactive than N-terminal amines, their high density and availability in the peptide chains could increase their possible reactivity during the reaction.
The inter-particle crosslinking could restrict the interaction of peptide chains with pDNA which resulted in less condensation observed in the electrophoresis assay. This is also in agreement with the previous study on TAT-immobilized gold nanoparticles (AuNPs) which reported the instability and aggregation of AuNPs with increasing TAT concentration up to 2 μg/mL [33]. Sterling et. al. has studies surface modification of Au nanoparticles by covalent conjugation of NH_2-PEG- NH_2 using EDC/NHS. They have reported the inter-particle crosslinking by increasing NH_2-PEG- NH_2 ratio to Au nanoparticle [34]. It can be assumed that the concentration of peptide can then strongly affect chains conjugation of GO nano-sheets and result in reduced conjugational efficacy duo to the partial intra-particle crosslinking.

The size of nano-carriers/plasmid complexes was evaluated using DLS after 30 min incubation of 1μg pEGFP with10 μg of GOP samples suspended in deionized water (Table 1). The increase in size of GOP0.5 and GOP1 upon complexation with pEGFP could be explained by electrostatic interaction between the negatively charged plasmid and positively charged GOP0.5 and GOP1 nano-carrier formulations. This could be justified to successful complexation and plasmid loading on these samples. As it was expected based on the zeta value for GOP0.1, there is no significant size increase after incubation with plasmid. In the case of GOP1.5/pDNA, the size distribution was variable and it is assumed that further incubation in presence of plasmid may trigger precipitation of the complexes.

3.7. Cytotoxicity assay

The viability of fibroblast cells (L929) treated by NGOS, R8, and GOPs in the absence of plasmid after 48 h incubation was determined by MTT assay. The results showed that cell viability remained above 85% even after the addition of 250 μg/mL NGOS. There was a reduction in cell viability after the addition of 10, 50, and 100 μg/mL of NGOS by 7.5, 11 and 10%, respectively, compared to the non-treated cells. However, the reduction in viability of cells was not statistically significant (Fig.6). It is known that the addition of CPPs at certain concentrations could enhance gene expression. However, these concentrations were mostly

increased the risk of cytotoxicity and immunogenicity [36]. To explore the optimum concentration of R8 peptide for conjugation to GO nano-sheets, four different concentrations of peptide were used. The MTT results showed the highest cell viability with the addition of 50 µg/mL R8 peptide. The addition of 100 µg/mL R8 peptide reduced the relative cell viability slightly compared to the other samples and significantly compared to the control. The conjugation of R8 to NGOS showed no cell toxicity even after the addition of 250 µg/ml of nano-carriers. By varying conjugation ratio of peptide to NGOS, no significant cytotoxicity was detected after incubation of L929 cells with GOPs at the concentration of 100 µg/mL. All the samples with various conjugation ratios of peptide presented comparable cell viabilities to the non-treated sample used as control. However, PEI treated cells at the same concentration with GOPs (100 µg/ml) showed significant decrease in cell viability compared to the control. In addition, light microscopy images revealed similar morphology for the cells treated with R8-NGOS and un-treated ones. (Fig.7).These results suggested that the peptide modified NGOS was not cytotoxic in any of concentrations being used and had no apparent effect on proliferation inhibition of the cells.

3.8. Gene transfection

3.8.1. Gel retardation assay

For successful gene delivery a gene carrier that interacts with genetically materials such as pDNA generally through electrostatic interaction is essential. The NGOS possess surface negative charges and inherently does not interact with pDNA with a negatively charged phosphate backbone. It is crucial to modify the NGOS with cationic peptides like R8 in order to acquire more positive surface charge and enable the formation of nano-complex with pDNA. The formation of nano-complexes which consist of nano-carriers and pDNA was examined by agarose gel electrophoresis. As depicted in Fig 8a, the peptide functionalized NGOS strongly condensed pDNA more clearly for GOP0.5 and GOP1. In the GOP1.5 it seems that the bonded peptide chains were not enabled to interact with pDNA and retard migration. It was also revealed that the migration of pDNA completely was retarded when the R8 concentration was more than 1 µg/mL (Fig. 8b) whereas none of the NGOS concentrations could retard pDNA migration under applied electrical field (Fig. 8c). According to zeta potential results, GOP1 and GOP1.5 showed the most positively charged surfaces among the peptide functionalized samples, therefore, it is expected that they could efficiently form complexes with pDNA and retard migration. However, the negatively charged GOP0.1 and GOP0.5 also showed plasmid retardation ability. Similar observations was previously reported by Sanz et al. regarding siRNA loading on gold nano-particles modified with TAT cell penetration peptide. This phenomenon cannot be purely explained by the electrostatic interactions between positive charges of peptide and negative charges of phosphate in DNA. It is assumed that some hydrogen bonding may be formed between amide groups (peptide bond) and hydroxyl group in ribose groups of DNA. This could be the reason that the week negatively charged GOP nano-sheets showed a strong pDNA complexion and retardation. Although GOP1.5 showed higher conjugated peptide per mg of NGOS, GOP1 showed the most condensed pDNA. This could be another confirmation for the fact that peptide chains in GOP1.5 are not free enough to interact with plasmids duo to inter-particle crosslinking.

3.8.2. Transfection assay

The ability of the GOPs as gene vector to transfer pEGFP into the HEK cells was evaluated by fluorescence microscopy. The PEI 10^4Da/pDNA and R8/pDNA binary complexes with similar concentrations were used as controls. The fluorescent intensity of the transfected cells was correlated to the transfection efficiency. It was found that naked pEGFP and NGOS-pDNA failed to result EGFP expression in the HEK cells. Among peptide conjugated samples, GOP1 showed the most efficient delivery of the pEGFP into the treated cells and highest gene expression after 48 h incubation (Fig. 9). The cells treated with the GOP1 sample exhibited much stronger fluorescence intensity than those transfected with naked R8 while the GOP1.5 showed slight aggregation during incubation. Although the PEI transfected cells expressed EGFP, most of the cells were found nonviable duo to its cytotoxicity. It was concluded that the maximum transfection efficiency could be achieved using peptide to GO ratio of 1μmol:1mg (GOP1).

Quantitative assessment of transfection ability of samples based on fluorescent intensity of expressed GFP in presence and absence of serum protein was performed and compared with JetPEI® as a commercial transfection reagent. Based on the manufacture's protocol, JetPEI® was used in the presence of serum. The results showed GOP0.5 and GOP1 provide higher transfection ability (51% and 72%, respectively) rather than two other GOP formulations (Fig. 9). This is consistent with pDNA condensation assay observed with gel electrophoresis. The transfection efficacy showed a slight decline in presence of FBS, however; this decrease was not significant for any of GOP0.5 and GOP1. In the presence of FBS the transfection ability of GOP1.5 decreased 7 times which is evidenced by the instability observed during incubation with cell culture media (Fig. 9d). Even though the transfection ability of GOP1 was lower than that of Jet PEI®, it was the most efficient sample and considered the optimized R8-functionalized NGOS sample for gene delivery applications.

4. Summary and conclusion

Cell-penetrating peptides (CPPs) have gained much attention in recent years due to their ability to translocate drugs, genes, and large therapeutic molecules. One commonly used CPP group is polyarginine. The efficient cell-penetrating characteristic of polyarginine is related to rich domain residues of arginine that interacts with negatively charged proteoglycans on the cell membrane. In this study R8 was utilized to modify the graphene oxide surface to be used as an efficient gene delivery carrier. The influences of R8 conjugation ratio on the synthesized nano-graphene oxide particle size and surface charge as well as peptide conjugation density as important factors in cellular uptake were investigated. The R8-NGOS sample with peptide molar ratio of 1 μmol per mg of GO showed to be the most efficient and biocompatible gene delivery vehicle having desirable properties such as strong positive charge and good stability in aqueous solutions. It was also suggested that increasing peptide molar ratio from 1 to 1.5 μmol/mg may trigger inter-particle crosslinking via peptide chains which resulted in partial instability and nano-particles agglomeration. The optimized R8-NGOS sample showed efficient plasmid condensation, EGFP expression and high cell viability compared to PEI which is recognized as the 'golden standard' cationic polymer for gene transfection. The promising results altogether imply the potential of optimized R8-functionalized system as efficient non-viral gene delivery nano-carrier for gene therapy applications. However, the future studies should be directed toward increasing the stability of peptide functionalized NGOS in higher peptide conjugation ratios while avoiding inter-particle peptide crosslinking.

Acknowledgments

The authors wish to thank financial supports provided for this work by National Institute of Genetic Engineering and Biotechnology (NIGEB). We also gratefully acknowledge the scientific help and guidance of Hojatollah Vali, Mahdi Amrollahi and Mohammad Hasan Mohammadzadeh.

References:

1. T. Niidome and L. Huang, *Gene therapy*, 2002, 9, 1647-1652.
2. L. De Laporte, J. Cruz Rea and L. D. Shea, *Biomaterials*, 2006, 27, 947-954.
3. A. Lam and D. Dean, *Gene therapy*, 2010, 17, 439-447.
4. N. Sanvicens and M. P. Marco, *Trends in biotechnology*, 2008, 26, 425-433.
5. Z. Liu, S. Tabakman, K. Welsher and H. Dai, *Nano research*, 2009, 2, 85-120.
6. S.-r. Ji, C. Liu, B. Zhang, F. Yang, J. Xu, J. Long, C. Jin, D.-l. Fu, Q.-x. Ni and X.-j. Yu, *Biochimica et Biophysica Acta (BBA) - Reviews on Cancer*, 2010, 1806, 29-35.
7. V. Singh, D. Joung, L. Zhai, S. Das, S. I. Khondaker and S. Seal, *Progress in Materials Science*, 2011, 56, 1178-1271.
8. Y. Zhu, S. Murali, W. Cai, X. Li, J. W. Suk, J. R. Potts and R. S. Ruoff, *Advanced Materials*, 2010, 22, 3906-3924.
9. V. C. Sanchez, A. Jachak, R. H. Hurt and A. B. Kane, *Chem Res Toxicol*, 2012, 25, 15-34.
10. X. Sun, Z. Liu, K. Welsher, J. T. Robinson, A. Goodwin, S. Zaric and H. Dai, *Nano research*, 2008, 1, 203-212.
11. Y. Wang, Z. Li, J. Wang, J. Li and Y. Lin, *Trends Biotechnol*, 2011, 29, 205-212.
12. Z. Liu, J. T. Robinson, X. Sun and H. Dai, *Journal of the American Chemical Society*, 2008, 130, 10876-10877.
13. B. Chen, M. Liu, L. Zhang, J. Huang, J. Yao and Z. Zhang, *Journal of Materials Chemistry*, 2011, 21, 7736-7741.
14. L. Feng, S. Zhang and Z. Liu, *Nanoscale*, 2011, 3, 1252-1257.
15. H. Dong, L. Ding, F. Yan, H. Ji and H. Ju, *Biomaterials*, 2011, 32, 3875-3882.
16. L. Feng, S. Zhang and Z. Liu, *Nanoscale*, 2011, 3, 1252-1257.
17. H. Kim, R. Namgung, K. Singha, I.-K. Oh and W. J. Kim, *Bioconjugate chemistry*, 2011, 22, 2558-2567.
18. H. Bao, Y. Pan, Y. Ping, N. G. Sahoo, T. Wu, L. Li, J. Li and L. H. Gan, *Small*, 2011, 7, 1569-1578.
19. X. Yang, G. Niu, X. Cao, Y. Wen, R. Xiang, H. Duan and Y. Chen, *Journal of Materials Chemistry*, 2012, 22, 6649-6654.
20. M. Mae and U. Langel, *Curr Opin Pharmacol*, 2006, 6, 509-514.
21. R. M. Johnson, S. D. Harrison and D. Maclean, in *Cell-Penetrating Peptides*, Springer, 2011, pp. 535-551.
22. F. Shiroh, *International Journal of Pharmaceutics*, 2002, 245, 1-7.
23. D. M. Copolovici, K. Langel, E. Eriste and U. l. Langel, *ACS nano*, 2014, 8, 1972-1994.
24. H. Yukawa, Y. Kagami, M. Watanabe, K. Oishi, Y. Miyamoto, Y. Okamoto, M. Tokeshi, N. Kaji, H. Noguchi and K. Ono, *Biomaterials*, 2010, 31, 4094-4103.
25. W. Hummers and R. Offeman, *J Am Chem Soc*, 1958, 80, 1339-1345.
26. J. Shen, M. Shi, B. Yan, H. Ma, N. Li, Y. Hu and M. Ye, *Colloids and Surfaces B: Biointerfaces*, 2010, 81, 434-438.
27. L. Zhang, J. Liang, Y. Huang, Y. Ma, Y. Wang and Y. Chen, *Carbon*, 2009, 47, 3365-3368.
28. W. Davis, C. Erickson, C. Johnston, J. Delfino and J. Porter, *Chemosphere*, 1999, 38, 2913-2928.
29. T. Szabó, E. Tombácz, E. Illés and I. Dékány, *Carbon*, 2006, 44, 537-545.
30. H. Kim and W. J. Kim, *Small*, 2014, 10, 117-126.
31. Q. Yang, X. Pan, K. Clarke and K. Li, *Industrial & Engineering Chemistry Research*, 2011, 51, 310-317.
32. R. Foldbjerg, E. S. Irving, J. Wang, K. Thorsen, D. S. Sutherland, H. Autrup and C. Beer, *Toxicology Research*, 2014.
33. V. Sanz, J. Conde, Y. Hernández, P. V. Baptista, M. Ibarra and M. Jesús, *Journal of Nanoparticle Research*, 2012, 14, 1-9.

34. R. A. Sperling, T. Pellegrino, J. K. Li, W. H. Chang and W. J. Parak, *Advanced Functional Materials*, 2006, 16, 943-948.
35. I. A. Khalil, K. Kogure, S. Futaki and H. Harashima, *Journal of Biological Chemistry*, 2006, 281, 3544-3551.
36. K. Saar, M. Lindgren, M. Hansen, E. Eiríksdóttir, Y. Jiang, K. Rosenthal-Aizman, M. Sassian and Ü. Langel, *Analytical biochemistry*, 2005, 345, 55-65.

Figure Captions

Table 1. Zeta potential and DLS particle size analyses. For zeta potential value and particle size (-pDNA), * *p*-value<0.005 compared to NGOS-COOH and ** *p*-value<0.001 compared to the other samples and control. For particle size analysis (+pDNA), * *p*-value<0.005 and ** *p*-value<0.001compared to the particle size before pDNA condensation and ** *p*-value<0.001compared to other samples.

Table 2. The quantification of conjugated peptide and reaction efficacy on the NGOS based on TNBS assay. * *p*-value<0.005 compared to the other samples.

Table 3. DLS particle size analysis after incubation in cell culture medium and DI water for 1 and 48 h. * *p*-value<0.005 compared to the particle size after 1 h incubation.

Schematic 1. A representation of structure and main functional groups of (a) GO (b) octaarginine (R8).

Schematic 2. A representation of TNBS assay for quantification of amine groups' molarity per mg of R8-NGOS.

Figure 1. FTIR spectra of NGOS, NGOS-COOH and R8- functionalized NGOS.

Figure 2. Size and morphological characterization of synthesized NGOS, NGOS-COOH and R8-NGOS: AFM image of (a) NGOS (b) carboxylated GO and (c) R8-NGOS (GOP1). The TEM image of (d) as-prepared NGOS (up) chloroacetic acid treated NGOS (down). The arrows show a NGOS-COOH single nano-sheet.

Figure 3. Uv-vis spectra of (a) NGOS and carboxylated NGOS in aqueous solution (b) R8 and R8-NGOS (all samples concentration was 0.01 mg/mL). (c) The XRD patterns of NGOS, NGOS-COOH and R8-NGOS.

Figure 4. The dispersibility and colloidal stability of peptide-functionalized samples: (a) after 48h incubation at room temperature (b) after 6h incubation with cell culture media supplemented with FBS at 37˚C.

Figure 5. Absorption peaks of TNBS solution after reaction with different concentrations of R8. The inset shows the calibration curve that presents the relation between absorbance and concentration at 345nm.

Figure 6. Histogram represents cell viability based on MTT assay for NGOS and R8 at different concentrations as well as R8-functionalized NGOS with various peptide conjugation ratios (100µg/mL). All samples compared to control (non-treated cells) * p <0.05 and ** p<0.005.

Figure 7. Optical microscopic images of L929 cells morphology of none treated cells (a) after 24h and (b) 48 h in comparison with cells incubated with GOP1 (c) after 24 h (d) 48 h.

Figure 8. Agarose gel retardation assay of pEGFP complexed with (a) R8-conjugated samples, (b) R8 and (c) NGOS.

Figure 9. The HEK293 cell line treated with GOP1-pEGFP complex after 48 h (a) transmission image (b) fluorescent image and (c) merged images. Quantification of transfection ability after 48 h of cell transfection in presence and absence of FBS (d). * *p*-value<0.005 compared to transfection ability in the absence of FBS.

Table 1. Zeta potential and DLS particle size analyses. For zeta potential value and particle size (-pDNA), * *p*-value<0.005 compared to NGOS-COOH and ** *p*-value<0.001 compared to the other samples and control. For particle size analysis (+pDNA), * *p*-value<0.005 and ** *p*-value<0.001compared to the particle size before pDNA condensation and ** *p*-value<0.001compared to other samples.

Sample	Zeta potential value(mv)	Particle size analysis (- pDNA)		Particle size analysis (+ pDNA)	
		Effective diameter (nm)	PDI	Effective diameter (nm)	PDI
NGOS	-35±1.5	110±6	0.002±0.001	-	-
NGOS-COOH	-46±0.8	85±2.5	0.005±0.001	-	-
GOP0.1	-33±1.7	95±3.1	0.011±0.007	101±5.1	0.1±0.014
GOP0.5	-7±0.1*	123±13*	0.100±0.014	195±7.2*	0.23±0.009
GOP1	+23±0.4*	168±18*	0.050±0.008	277±6.4*	0.29±0.031
GOP1.5	+31±2.2*	322±20*	0.37±0.065**	550± 87*	0.45±0.08**

PDI: Polydispersity index

Table 2. The quantification of conjugated peptide and reaction efficacy on the NGOS based on TNBS assay. * *p*-value<0.005 compared to the other samples.

Sample	**Conjugated-R8 (μmol/mg)**	**Estimated Number of R8 molecules per 1 mg of NGOS (× 10^{-15})**	**Conjugation Efficacy%**
GOP0.1	0.007±0.003	4.2	7.00
GOP0.5	0.041±0.001	24.6	8.20
GOP1	0.134±0.009*	80.4	13.40*
GOP1.5	0.18±0.015*	108.0	12.00*

Table 3. DLS particle size analysis after incubation in cell culture medium and DI water for 1 and 48 h. * *p*-value<0.005 compared to the particle size after 1 h incubation.

Sample	Effective diameter (nm) in DMEM		Effective diameter (nm) in deionized water	
	After 1h incubation	After 48h incubation	After 1h Incubation	After 48h incubation
GOP0.1	110±2.2	119±9.2	98±0.7	119±9.2
GOP0.5	132±9.3	140±11.2	127±4.3	140±11.2
GOP1	188±8.1	196±8.5	172±11	196±8.5
GOP1.5	388±33	> 1μm*	330±14	797±112*

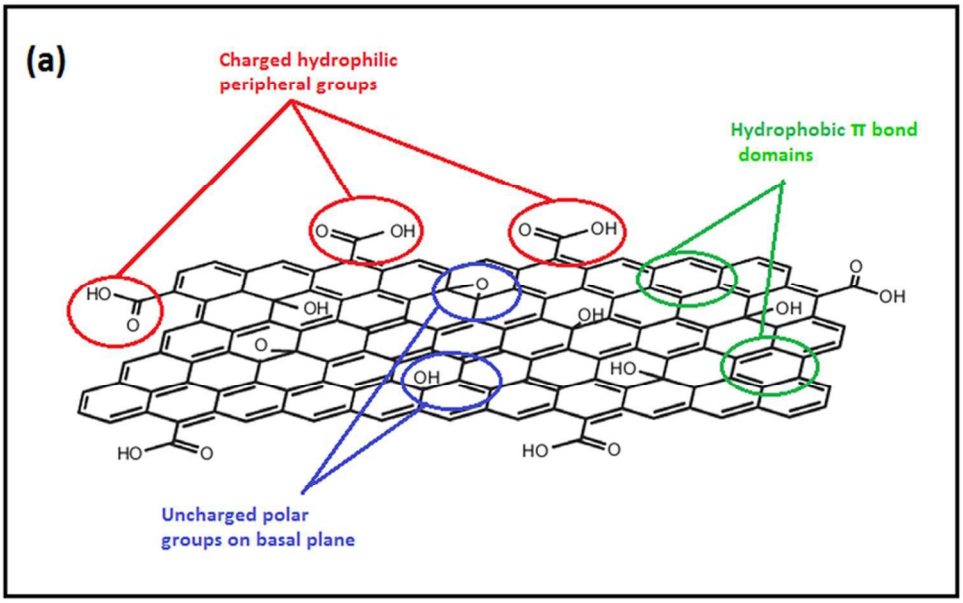

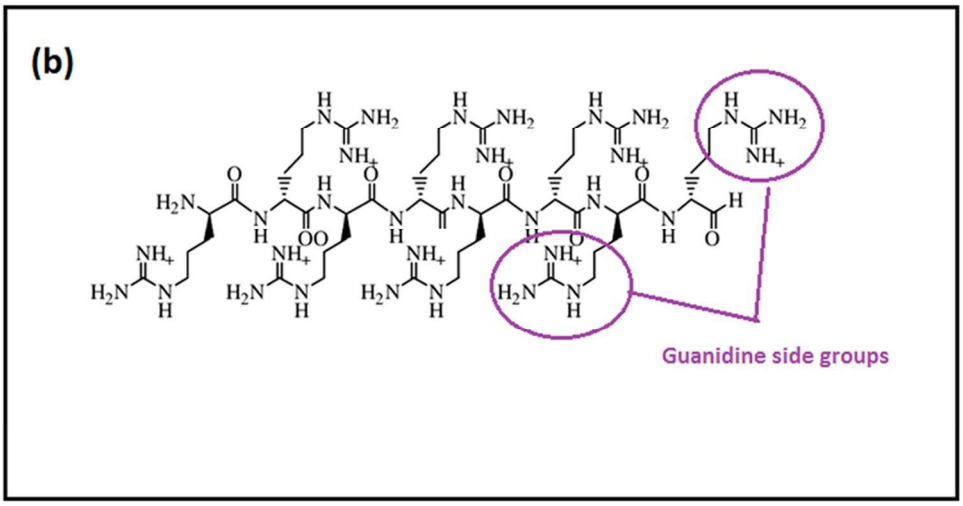

96x116mm (300 x 300 DPI)

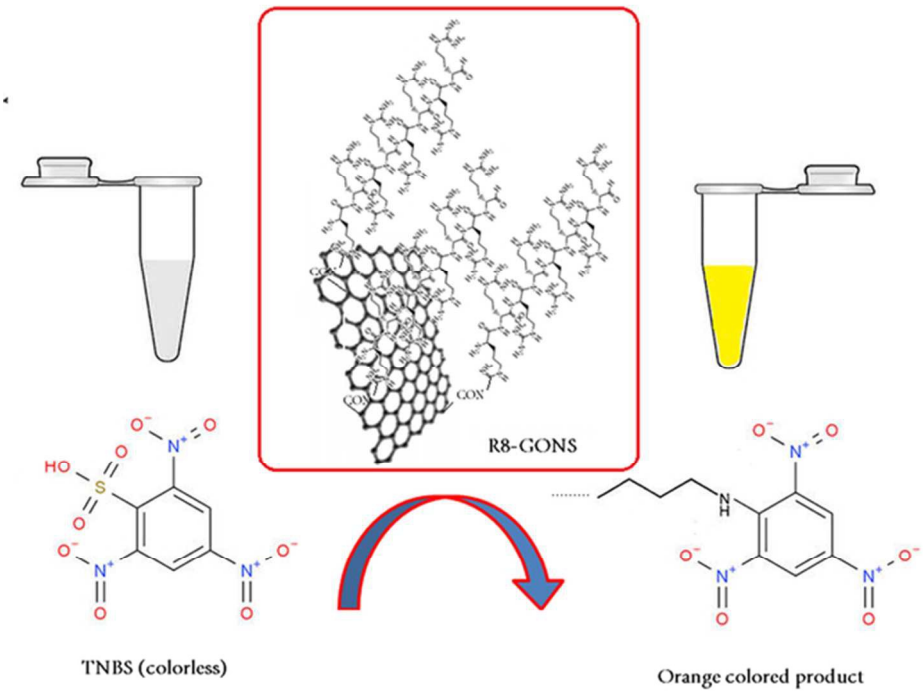

61x46mm (300 x 300 DPI)

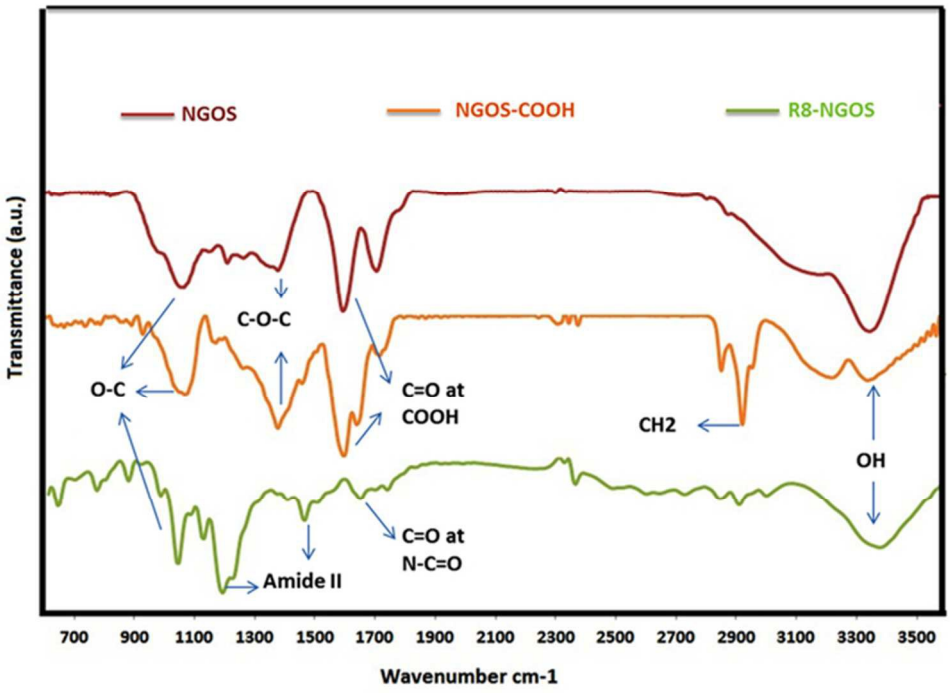

57x40mm (300 x 300 DPI)

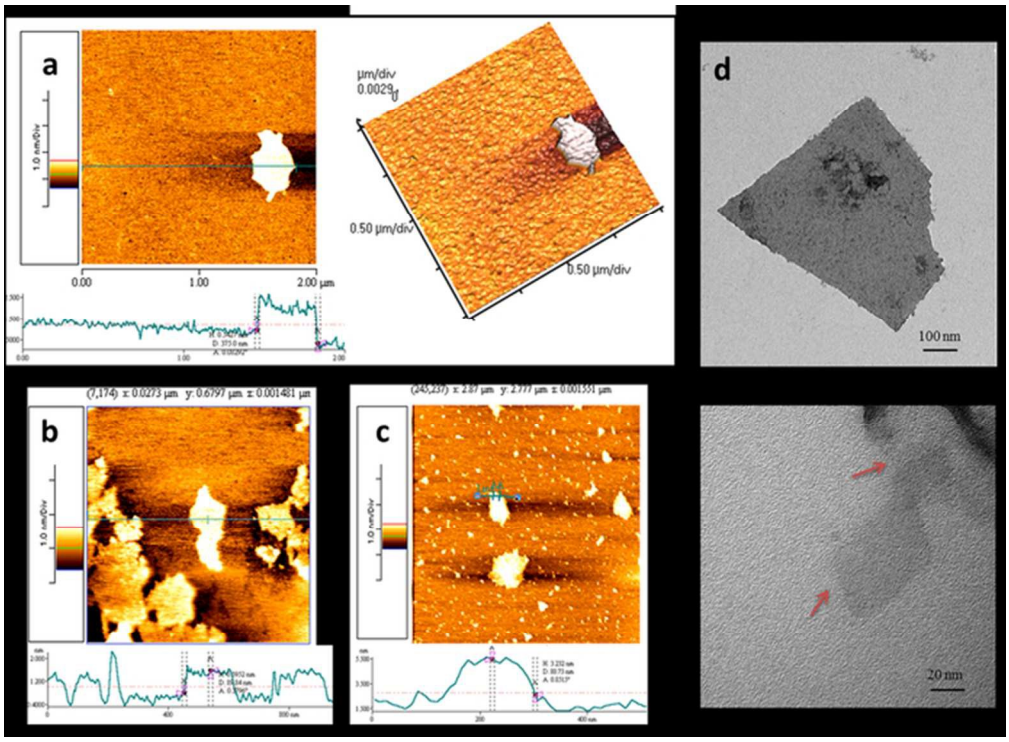

58x42mm (300 x 300 DPI)

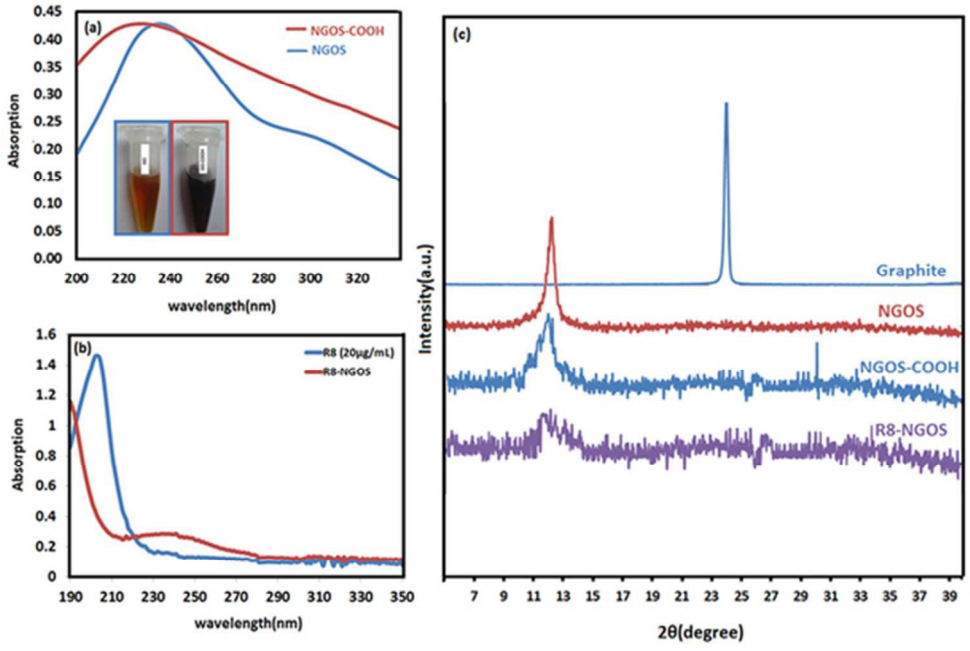

53x35mm (300 x 300 DPI)

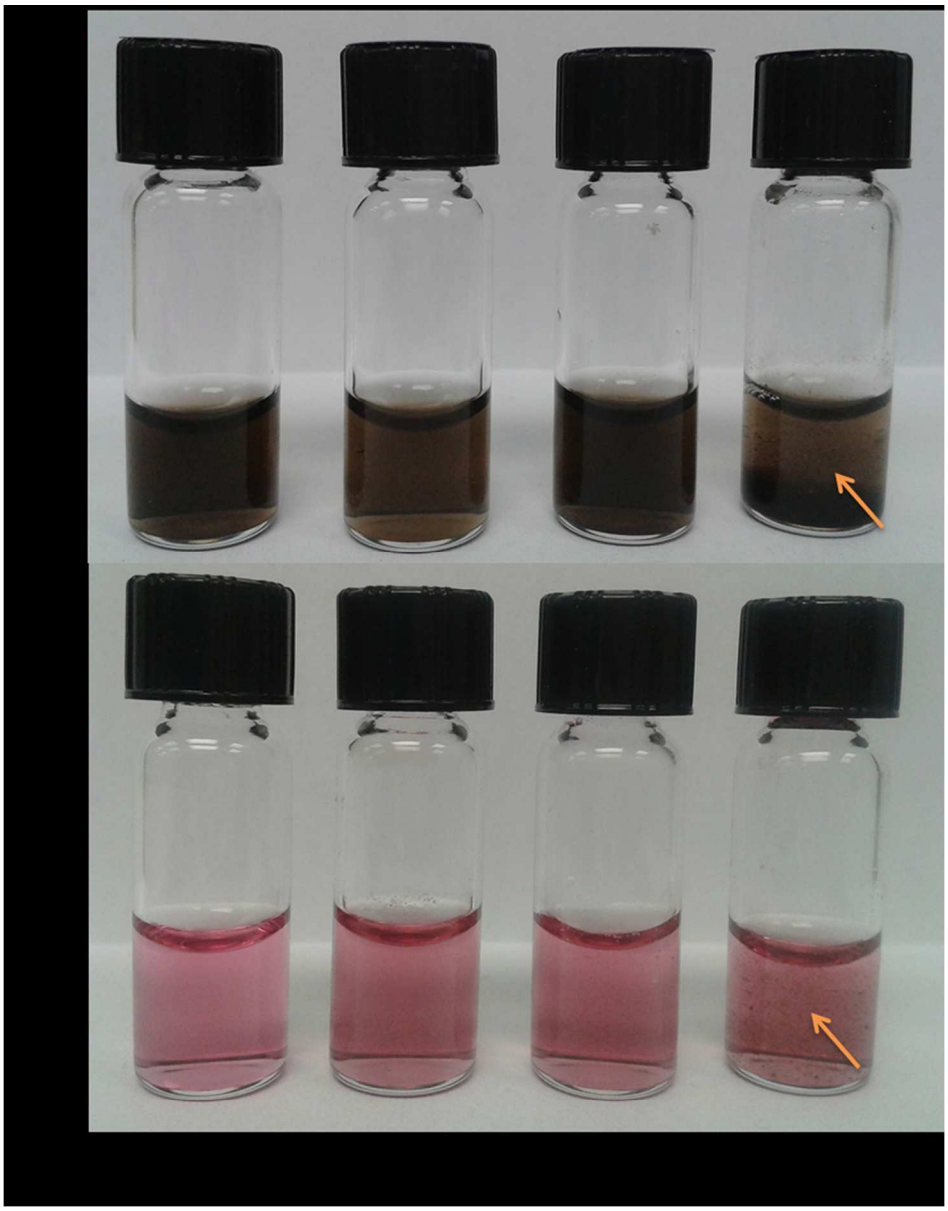

102x130mm (300 x 300 DPI)

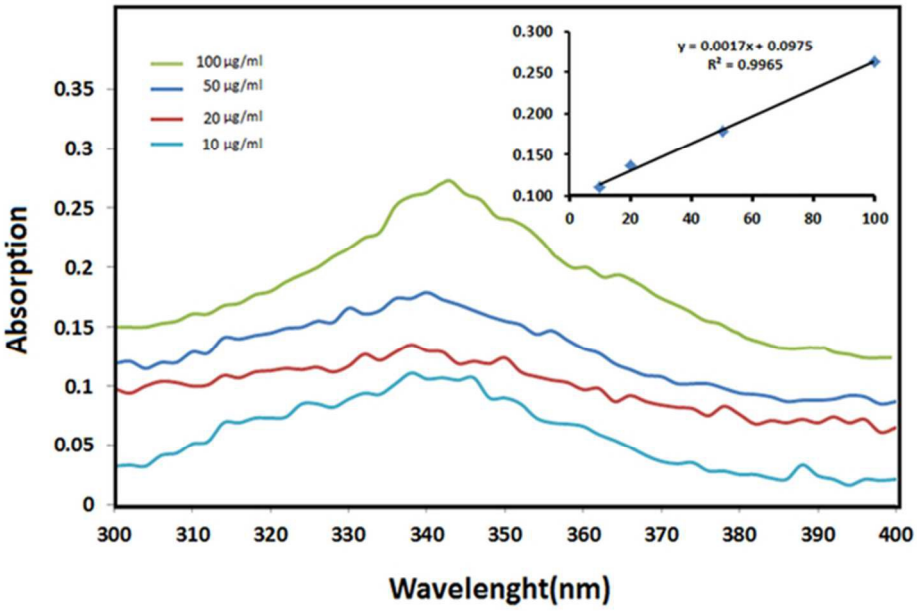

55x39mm (300 x 300 DPI)

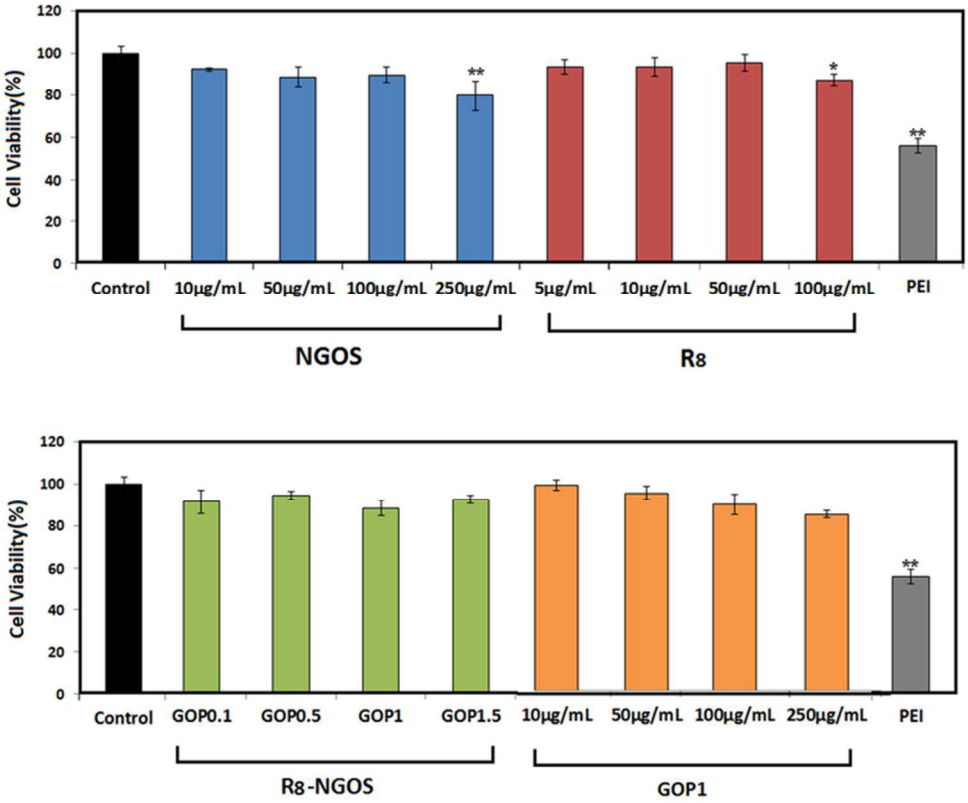

65x53mm (300 x 300 DPI)

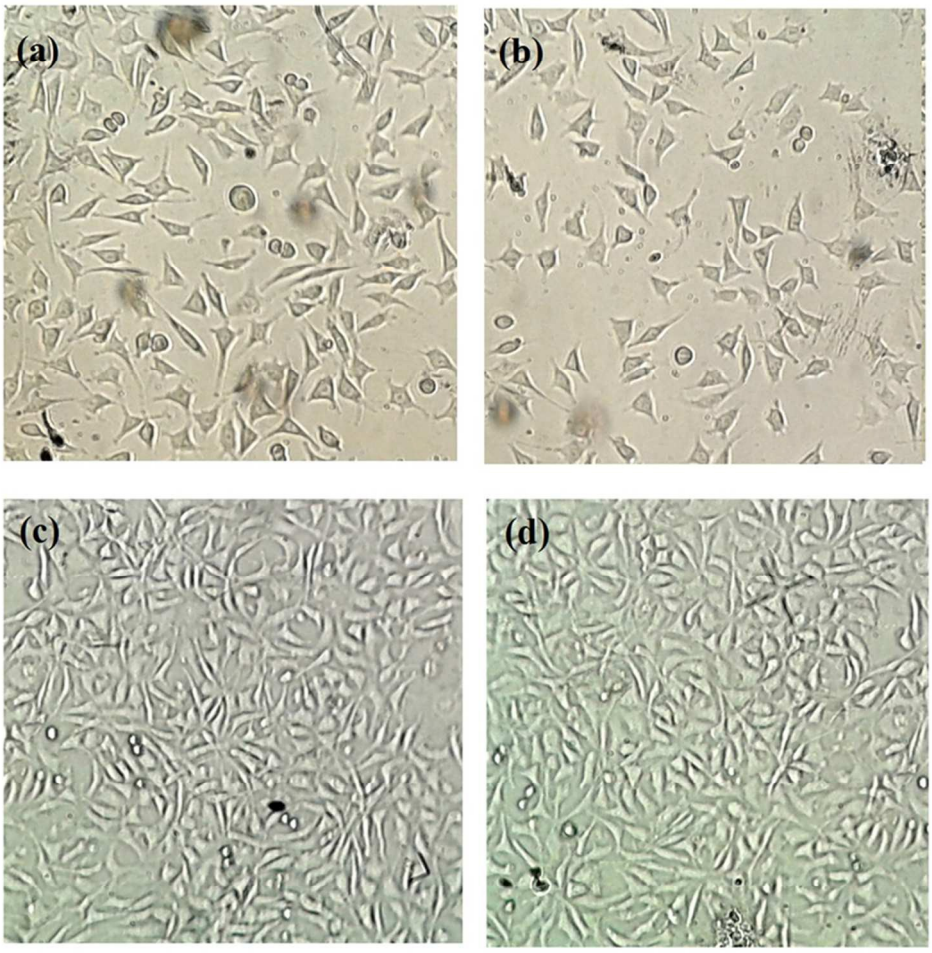

82x85mm (300 x 300 DPI)

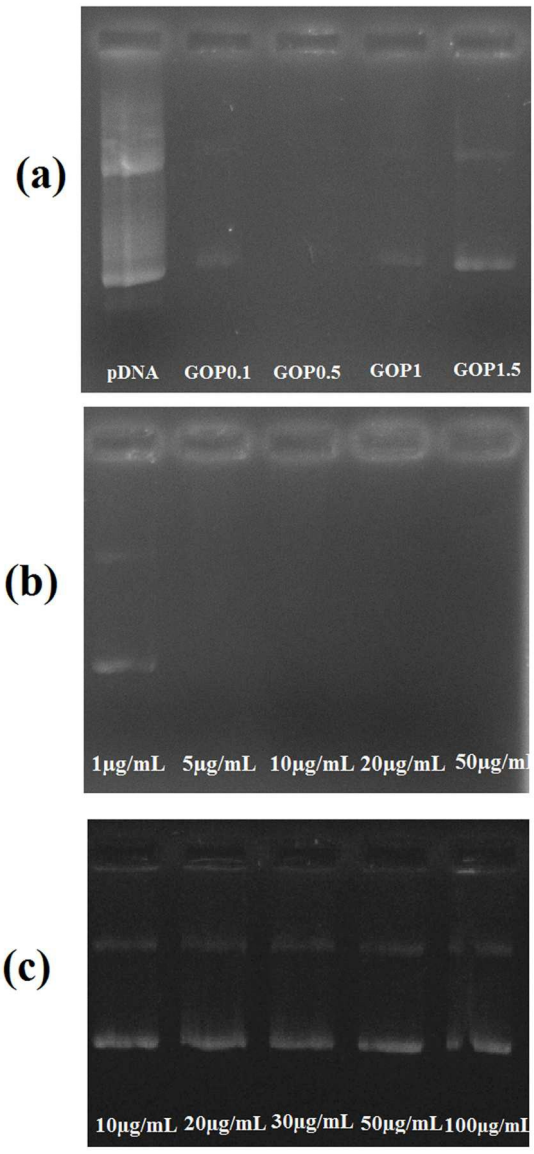

168x354mm (300 x 300 DPI)

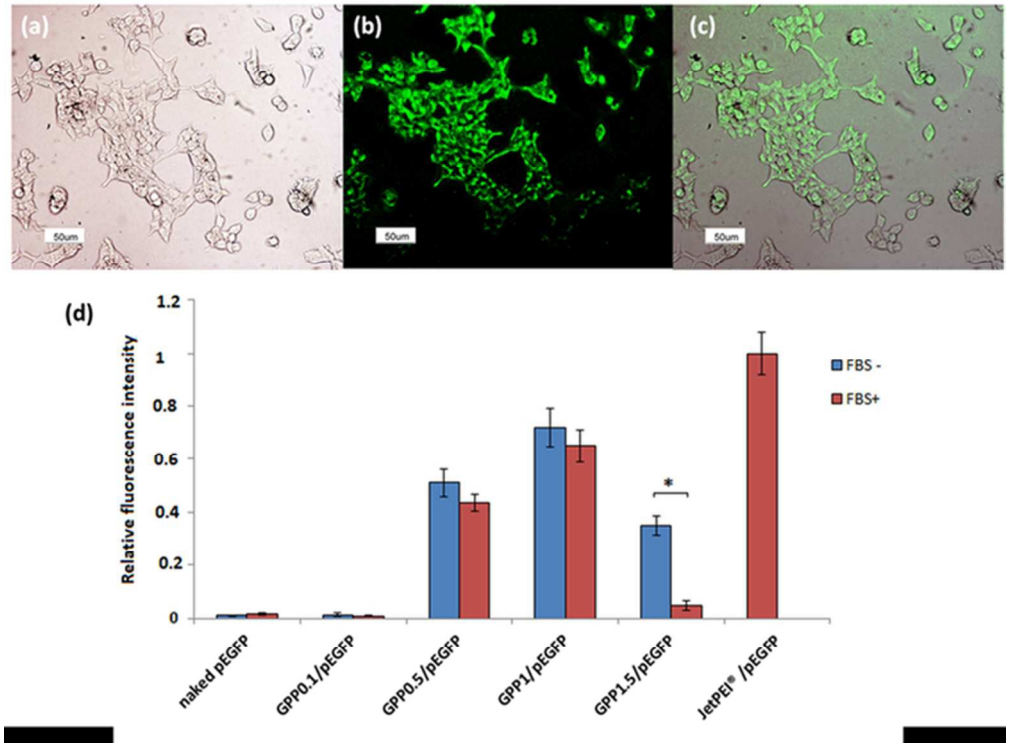

61x46mm (300 x 300 DPI)